Proton Compton scattering in a unified proton-Δ^+ model

Yun Zhang and Konstantin Savvidy
Department of Physics, Nanjing University, Nanjing, China
(Received 12 June 2013; revised manuscript received 22 October 2013; published 26 December 2013)

We develop a field-theoretic model for the description of the proton Compton scattering in which the proton and its excited state, the Δ^+ resonance, are described as parts of one multiplet with a single Rarita-Schwinger wave function. To describe the observed phenomena, it is necessary to incorporate both minimal and nonminimal couplings. The minimal coupling reflects the fact that the Δ^+ is a charged particle, and in this model the minimal coupling contributes also to the $\gamma N\Delta$ magnetic transition. The nonminimal couplings consist of five electromagnetic form factors, which are accessed at fixed and vanishing momentum transfer squared with real photons in the Compton scattering experiments, therefore it is possible to extract a somewhat well-determined set of optimal parameters which fit the data in the resonance region 140–450 MeV reasonably well. The crucial parameter which determines the $\gamma N\Delta$ transition amplitude and therefore the height of the resonance peak is equal to 1.83 ± 0.03, in units of μ_N. We find that this parameter is also the primary determinant of the contributions to the magnetic polarizability in this model. In the low-energy region up to 140 MeV, we separately fit the electric and magnetic polarizabilities while keeping the other parameters fixed, and obtain values in line with previous approaches. In addition to proton Compton scattering, the model is applicable to a broad range of processes in the few hundred MeV energy range, whenever the proton appears in some intermediate off-shell state.

DOI: 10.1103/PhysRevC.88.064614 PACS number(s): 12.39.Fe, 13.40.Gp, 13.60.Fz, 14.20.Dh

I. BACKGROUND AND INTRODUCTION

The proton is the particle which makes up the greatest fraction of matter in the visible universe and its properties have been studied extensively. Nevertheless it still holds some mysteries, among them the physical origin of the electric and magnetic polarizabilities. The polarizabilities are important electromagnetic properties of the proton, and appear at the next order in the expansion of the amplitudes in powers of energy, right behind the more fundamental properties such as the electric charge and the magnetic moment. Experiments have been done since the 1960s to characterize and measure the electromagnetic properties of the proton using fixed-target Compton scattering [1–6]. In the last two decades, high-quality proton Compton scattering data in the first $\Delta(1232\text{MeV})$ resonance region have been obtained at the Saskatchewan Accelerator Laboratory [7], by the LEGS collaboration [8] and by MAMI at Mainz [9,10]. Recent high-quality data have also become available in the higher energy region, from the experiments by Hall A Collaboration at the Jefferson Lab [11].

These most recent and precise experiments have determined the static values of the electric and magnetic polarizabilities; see, for example [12,13]. In particular, the sign and value of the magnetic polarizability have been measured; these remained shrouded in uncertainty for a long time. Additional experiments to measure the polarizabilities even more precisely were proposed recently in Ref. [14]. In addition, a high precision value was obtained for the forward spin polarizability [9,10] which appears in the expansion of the scattering amplitudes to the third order in momentum. Upcoming experiments will soon measure all the spin polarizabilities using polarized beams and targets.

Experimentally, it is certainly possible to measure the polarization asymmetries as a function of the angle and energy, for example, in the last experiment done at the venerable Yerevan accelerator [15] and in the first resonance region by the LEGS collaboration [16]. These data can be used to discriminate theoretical models as a strong cross-check, once the basic parameters of the model have been well determined.

The process in the low photon energy range up to 140 MeV is dominated by contributions from the anomalous magnetic moment as well as the polarizabilities of the nucleon. Of these additional contributions, the anomalous magnetic moment contributes to the amplitude already at the linear order while the polarizabilities start out at the second order, thus the cross section can grow at first quadratically and then quartically with energy. This is in contrast to the minimal coupling in QED, where the Klein-Nishina cross section is essentially flat in the relevant energy range.

Fundamental results on the scattering of light by particles of spin $1/2$ with an anomalous magnetic moment were obtained by Powell, Low, Gell-Mann, and Goldberger [17–19]. Early theoretical progress was driven by the phenomenologically very successful dispersion theory approach [20–31]; see also the latest excellent review in Ref. [32]. This approach was supplemented by the insights gained from considering the pion-vertex corrections and a multitude of other improvements such as those in Refs. [13,33–36].

On the other hand, within the purely field-theoretic chiral-Lagrangian paradigm [37,38], the development of a promising approach of Peccei [39,40] was held up by difficulties in the field theory of the spin $3/2$ Δ^+ particle. The most egregious of these pathologies have been resolved in Ref. [41]. This better understanding of the theoretical requirements on the Δ propagator led to the paper of Pascalutsa and Scholten [42] in which the first workable field-theoretical model for the proton Compton scattering incorporating the contribution of the resonance was constructed. There, it was argued that the virtual spin $1/2$ degrees of freedom present in the standard

propagator do play a role in the Compton scattering amplitude. As we shall see, the present work's approach most directly descends from this model of Pascalutsa and Scholten and the subsequent recent developments in Refs. [43–51].

A separate development was the proposal to rid the theory of spin 3/2 particles of pathologies that stem from superluminal solutions by Ranada and Sierra in Ref. [52]. There, it was found that taking a Rarita-Schwinger multiplet of a physical spin 3/2 particle and a physical spin 1/2 particle (with different masses), would result in an acceptable wave equation even when minimally coupled to the electromagnetic field. A detailed investigation of the structure of poles in the propagator revealed that additional restrictions on the Ranada and Sierra equations result in a unitary theory with positive definite residues at the Feynman poles, taking into account the locations of the poles above or below the real axis [53].

In the present paper we make use of the propagator of [53], in combination with the observation of Pascalutsa and Scholten that the spin 1/2 degrees of freedom may be from another baryon, and propose a model where this spin 1/2 mode is interpreted as the proton, such that the proton and the Δ^+ are together described by a single multicomponent wave function of Rarita and Schwinger. The Δ^+ has the same quark constitution (uud) as the proton and is only slightly, less than 300 MeV, heavier than the proton. The only difference between the Δ^+ and the proton is the alignment of the spins of these quarks. In the proton, the d-quark spin is antialigned and makes the total proton spin $\frac{1}{2}$, while in the Δ^+ all three quarks are aligned, making the Δ^+ spin $\frac{3}{2}$. This makes it very natural to consider the possibility of a unified description; see Sec. II for the Lagrangian and more details.

This hypothesis confers several benefits. Low-energy proton Compton scattering occurs mainly through the exchanges of the proton and the Δ^+ in the s and u channels and the exchanges of pions in the t channel; see Fig. 1. The $\Delta^+(1232\ \text{MeV}, J^P = \frac{3}{2}^+)$, the lightest baryon resonance, appears in the intermediate state. Furthermore, the Δ^+ is only slightly heavier than the proton, so that even at the lowest energies this contribution is not suppressed compared with that from the exchange of the proton alone. In our model, because of the unified description, the s/u-channel proton and Δ^+ contributions can be calculated simultaneously as in Figs. 1(a) and 1(b) instead of adding up the four separate contributions.

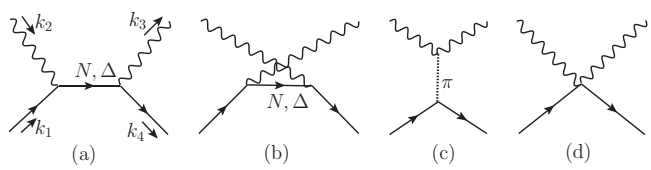

FIG. 1. The tree-level Feynman diagrams for the proton Compton scattering. In our model the propagator of the intermediate particle in the diagrams (a) and (b) contains the physical poles both for the proton and the Δ^+, and in (c) the π^0 meson is exchanged in the t channel. The diagram (d) is for the contact interaction in Eq. (13). For appropriate photon incident energy, the intermediate Δ^+ is approximately on-shell, and around this energy, there is the characteristic peak in the cross section which is dominated by the Δ^+ contribution.

The second benefit is that in this model it is possible to avoid the introduction of a large number of arbitrary parameters. In Sec. II A (see also [54]), we present in detail the five electromagnetic form factors which are possible for a spin 3/2 particle. These couple the momentum-independent fermion bilinears directly to the EM field strength. Three of these have clear physical interpretations as the magnetic moments of the proton and the Δ^+, and the strength of the $M1$ magnetic transition between the nucleon and the Δ^+. One of the remaining two parameters contributes a purely imaginary part to some amplitudes and this is disfavored by data, so that it can be safely set to zero (see Sec. VI).

In Sec. III, we discuss the γNN, $\gamma\Delta^+\Delta^+$, $\gamma N\Delta^+$ transition matrices and derive the formulas for the proton and the Δ^+ magnetic moments. In Sec. IV, we calculate the proton Compton scattering cross section and express the electric and magnetic polarizabilites in terms of the coefficients of the nonminimal interactions, and also present an analytic approximation to the amplitude around the Δ^+ pole. We fit the Compton scattering data in Sec. VI, and extract the polarizabilities using the expressions derived in Sec. IV. Because one linear combination of the coefficients of the nonminimal interactions gives the Δ^+ magnetic moment, our best-fit parameter set also provides a prediction of the Δ^+ magnetic moment, but we conservatively interpret it as an upper bound. The interactions in Sec. II A can also be used to calculate the $\Delta^+ \to N + \gamma$ decay width (Appendix A); this acts as a useful cross-check on our model.

II. LAGRANGIAN AND THE ELECTROMAGNETIC INTERACTIONS

A spin 3/2 field is represented as a field with both a Lorentz index and a Dirac index. The Lagrangian in Refs. [52,53] is

$$\begin{aligned} \mathcal{L} &= -\bar{\psi}_\lambda \left[p_\mu \, \Gamma^{\mu\lambda}_\rho - m \, \Theta^\lambda_\rho \right] \psi^\rho, \\ \Gamma^{\mu\lambda}_\rho &= \gamma^\mu \, \eta^\lambda_\rho + \xi \, (\gamma^\lambda \, \eta^\mu_\rho + \gamma_\rho \, \eta^{\lambda\mu}) + \zeta \, \gamma^\lambda \, \gamma^\mu \, \gamma_\rho, \\ \Theta^\lambda_\rho &= \eta^\lambda_\rho - z \, \gamma^\lambda \, \gamma_\rho, \\ \xi &= 2\,z - 1, \quad \zeta = 6\,z^2 - 4\,z + 1, \end{aligned} \tag{1}$$

in which the Dirac indices are suppressed. The solutions of the corresponding wave equation are all transverse, $p_\mu \, \psi^\mu = 0$, and consist of a spin 3/2 component with mass m and a spin 1/2 component with mass $M = \frac{m}{6z-2}$, compared to a pure spin 3/2 field in the original Rarita-Schwinger theory. We identify the spin 3/2 and 1/2 components as the Δ^+ and the proton, respectively, and thus unify them in one theory. This unification is very natural because the proton and the Δ^+ have the same quark constituents and both are dominated by configurations with all the quarks in the s wave. In addition, transition from one into the other is possible by absorbing or emitting a photon or even a neutral pion (which carries no charge or spin); this signifies that the two are states of the same physical system. The mass splitting between the nucleon and the Δ is less than 300 MeV. The model allows adjusting the z parameter to satisfy the observed ratio of the proton to the Delta mass.

The propagator with the specific arrangement of the poles is [53]

$$-i\,S(p) = \frac{(\not{p}+m)\,\Pi_3}{p^2-m^2+i\,\epsilon} - \frac{(\not{p}+M)\,\Pi_{11}}{p^2-M^2-i\,\epsilon}\,\frac{2M^2}{m^2} + [\Pi_{22}-(\Pi_{21}+\Pi_{12})/B+\Pi_{11}3/B^2]\frac{3}{2(M+2m)}, \quad B = \frac{3\,m}{2M+m}, \tag{2}$$

where the standard spin projection operators Π can be found, for example, in Ref. [41]. Note, that at high energies there is a destructive interference between the contributions of the virtual proton and Δ.

The minimal electromagnetic interaction is usually derived by substituting $p_\mu \to p_\mu + e\,A_\mu$. The interaction Lagrangian is

$$\mathcal{L}_I = e\,\bar{\psi}_\lambda\,\Gamma^{\mu\lambda}_\rho\,\psi^\rho\,A_\mu. \tag{3}$$

Ward identity is satisfied:

$$-i\,k_\mu\,\Gamma^{\mu\lambda}_\rho = S^\lambda_\rho(p+k)^{-1} - S^\lambda_\rho(p)^{-1}, \tag{4}$$

and as we shall see in the next subsection there are only a finite number of additional possibilities of electromagnetic couplings which satisfy gauge invariance and the Ward identity.

A. Nonminimal electromagnetic interactions

For a phenomenological application to the proton Compton scattering, the minimal interaction alone does not suffice. A well-known fact of Dirac theory is that it allows for two electromagnetic form factors, one of which is charge and the other describes the anomalous magnetic moment. We add the as yet undetermined nonminimal interactions to the vertex:

$$\tilde{\Gamma}^{\mu\lambda}_\rho = \Gamma^{\mu\lambda}_\rho + \frac{i}{2M}\sum_n F_n(k^2)\,(\Gamma_n)^{\mu\lambda}_\rho, \tag{5}$$

where the $F_n(k^2)$ are form factors. If the amplitudes are to be gauge invariant, the Ward identity (4) should still hold. For that to occur, it is sufficient to have $k_\mu(\Gamma_n)^{\mu\lambda}_\rho = 0$ and thus Γ_n should be of the form,

$$(\Gamma_n)^{\mu\lambda}_\rho = (\Sigma_n)^{\mu\nu\lambda}_\rho\,k_\nu, \tag{6}$$

where $(\Sigma_n)^{\mu\nu\lambda}_\rho$ is antisymmetric in μ and ν.

Antisymmetric tensors live in the $(1,0)\oplus(0,1)$ representation of the Lorentz group, and we can count the number of these representations in the product representation of the two matter fields. The representation for ψ_λ (or $\bar{\psi}_\lambda$) is a product of that for a vector field and that for a spinor field:

$$\left(\tfrac{1}{2},\tfrac{1}{2}\right)\otimes\left[\left(\tfrac{1}{2},0\right)\oplus\left(0,\tfrac{1}{2}\right)\right] = \left(1,\tfrac{1}{2}\right)\oplus\left(0,\tfrac{1}{2}\right)\oplus\left(\tfrac{1}{2},0\right)\oplus\left(\tfrac{1}{2},1\right). \tag{7}$$

The vertices live in the tensor product of the above reducible representations, and

$$\left[\left(1,\tfrac{1}{2}\right)\oplus\left(0,\tfrac{1}{2}\right)\oplus\left(\tfrac{1}{2},0\right)\oplus\left(\tfrac{1}{2},1\right)\right]\otimes\left[\left(1,\tfrac{1}{2}\right)\oplus\left(0,\tfrac{1}{2}\right)\oplus\left(\tfrac{1}{2},0\right)\oplus\left(\tfrac{1}{2},1\right)\right] \supset 5\,[(1,0)\oplus(0,1)]. \tag{8}$$

This tells us there are precisely five antisymmetric tensors and we have been able to explicitly construct them as

$$\begin{aligned}
(\Sigma_1)^{\mu\nu\lambda}_\rho &= -\frac{1}{2}\tau^{\mu\nu\lambda}_\rho,\\
(\Sigma_2)^{\mu\nu\lambda}_\rho &= \sigma^{\mu\nu}\eta^\lambda_\rho,\\
(\Sigma_3)^{\mu\nu\lambda}_\rho &= -\frac{1}{9}\gamma^\lambda\sigma^{\mu\nu}\gamma_\rho,\\
(\Sigma_4)^{\mu\nu\lambda}_\rho &= \frac{1}{12}\big(\gamma^\lambda\gamma^\mu\eta^\nu_\rho - \gamma^\lambda\gamma^\nu\eta^\mu_\rho + \gamma^\mu\gamma_\rho\eta^{\nu\lambda} - \gamma^\nu\gamma_\rho\eta^{\mu\lambda}\big),\\
\big(\Sigma_5\big)^{\mu\nu\lambda}_\rho &= \frac{-i}{12}\big(\gamma^\lambda\gamma^\mu\eta^\nu_\rho - \gamma^\lambda\gamma^\nu\eta^\mu_\rho - \gamma^\mu\gamma_\rho\eta^{\nu\lambda} + \gamma^\nu\gamma_\rho\eta^{\mu\lambda}\big),
\end{aligned} \tag{9}$$

where τ and σ are the generators of the Lorentz transformation for spin 1 and 1/2, respectively, $\tau^{\mu\nu\lambda}_\rho = i(\eta^{\mu\lambda}\eta^\nu_\rho - \eta^{\nu\lambda}\eta^\mu_\rho)$, and $\sigma^{\mu\nu} = \frac{i}{4}(\gamma^\mu\gamma^\nu - \gamma^\nu\gamma^\mu)$. The tensors listed above constitute just one economical choice, among the possible choices of the basis in the required five-dimensional linear space. The coefficients are normalized such that the form factors F_n enter with equal weights in the proton magnetic moment in Eq. (16).

These tensors satisfy the requirement of Hermiticity:

$$\big[\bar{\psi}(p_1)_\lambda\Sigma^{\mu\nu\lambda}_{n\rho}\psi^\rho(p_2)(p_1-p_2)_\nu\big]^\dagger = -\bar{\psi}(p_2)_\lambda\Sigma^{\mu\nu\lambda}_{n\rho}\psi^\rho(p_1)(p_2-p_1)_\nu, \tag{10}$$

which implies that the form factors $F_n(k^2)$ are real.

At higher order in momentum there are a small number of additional possibilities. The pure spin 3/2 field has three form factors other than charge [54], while only the first and second ones in Eq. (9) contribute for the spin 3/2 mode, because $\gamma_\rho\,\psi^\rho = 0$ for the spin 3/2 solutions. Thus we add one more tensor:

$$(\Sigma_6)^{\mu\nu\lambda}_\rho = \frac{1}{M^2}\,k^\lambda\,\sigma^{\mu\nu}\,k_\rho. \tag{11}$$

The form factors $F_n(k^2)$ which appear as the coefficients in Eq. (5) are scalar functions of the momentum transferred squared $k^2 = (p_1-p_2)^2$. For real Compton scattering and Delta decay $\Delta^+ \to p+\gamma$, the photons are on-shell $k^2 = 0$, so these form factors are taken to be constants in what follows.

B. Bare polarizability effective Lagrangian

Expanding the Compton scattering cross section at low energies, the static polarizabilities $\bar{\alpha}$ and $\bar{\beta}$ first enter at the second order:

$$\frac{d\sigma}{d\Omega_{\rm lab}} = \left(\frac{d\sigma}{d\Omega}\right)_{\rm Powell} - \frac{e^2\omega^2}{4\pi M}\left(\frac{\bar{\alpha}+\bar{\beta}}{2}(1+\cos\theta)^2 + \frac{\bar{\alpha}-\bar{\beta}}{2}(1-\cos\theta)^2\right) + \mathcal{O}(\omega^3). \tag{12}$$

Thus, the polarizabilities are defined here in the standard way in the literature, by comparing the theoretical predictions and the experimental data to the Powell cross section $(\frac{d\sigma}{d\Omega})_{\rm Powell}$, which is the differential cross section of the scattering of light

by a Dirac point particle with the anomalous magnetic moment included [17–19]. A different definition would result if the Klein-Nishina cross section for a Dirac point particle without an anomalous magnetic moment is taken as the basis for comparison. Such a difference has sometimes led to confusion in the literature, but was satisfactorily resolved by separating the contributions from the anomalous magnetic moment. Likewise, the nonminimal interaction vertices presented in this section contribute to the effective polarizabilities $\bar{\alpha}$ and $\bar{\beta}$ as we shall see in Sec. IV. In addition to these vertices, we may include also an effective four-point interaction that can contribute directly to the polarizabilities. Inspired by the effective Lagrangian proposed in Ref. [55], we include the following interaction Lagrangian to model the "bare" polarizabilities:

$$\mathcal{L}_{\rm pol} = \frac{i\pi}{M}\left(\bar{\psi}_\lambda\,\Gamma^{\mu\lambda}_{\rho}\,\partial_\nu\,\psi^\rho - \partial_\nu\,\bar{\psi}_\lambda\,\Gamma^{\mu\lambda}_{\rho}\psi^\rho\right) \times(\alpha_B F_{\mu\rho}\,F^{\rho\nu} + \beta_B \tilde{F}_{\mu\rho}\,\tilde{F}^{\rho\nu}). \tag{13}$$

This Lagrangian is not unique, but other candidates contribute identically to the cross section up to the second order in the energy of the incident photon.

The two coefficients α_B and β_B are the bare polarizabilities. The additional contribution of this effective Lagrangian to the laboratory frame Compton scattering amplitudes at second order in the photon energy is

$$\delta\mathcal{A} = 4\pi\,\alpha_B\,\omega\omega'\,\vec{\epsilon}\,'\cdot\vec{\epsilon} + 4\pi\,\beta_B\,\vec{\epsilon}\,'\times\vec{k}\,'\cdot\vec{\epsilon}\times\vec{k} + \mathcal{O}(\omega^3), \tag{14}$$

therefore it is a four-point contact interaction whose coupling constants are additive linearly to the polarizabilities via Fig. 1(d).

At higher orders in momentum it is possible to define and extract more general polarizabilities [56], such as the spin polarizabilities at the cubic order.

III. MAGNETIC MOMENTS AND THE $\gamma\,N\,\Delta^+$ TRANSITION MATRIX

To calculate the magnetic moments, we place the particles in a magnetic field by taking the (virtual) photon to be either left polarized $A^L = \frac{1}{\sqrt{2}}(0,1,i,0)$ or right polarized $A^R = \frac{1}{\sqrt{2}}(0,1,-i,0)$ and let $\vec{p}_1 - \vec{p}_2 = q\hat{z}$, with $\vec{p}_1 \to 0$, $\vec{p}_2 \to 0$,

$$\begin{aligned} &e\bar{u}_2(p_1,\sigma_1)\,\tilde{\Gamma}^\mu\,u_2(p_2,\sigma_2)\,A^L_\mu \\ &\quad= 2\,M\,\frac{\mu_p}{S_p}\left(J_+^{(\frac{1}{2})}\right)_{\sigma_1\sigma_2}(-iq) + \mathcal{O}(q^2), \\ &e\bar{u}_4(p_1,\sigma_1)\,\tilde{\Gamma}^\mu\,u_4(p_2,\sigma_2)\,A^L_\mu \\ &\quad= -2\,m\,\frac{\mu_{\Delta^+}}{S_{\Delta^+}}\left(J_+^{(\frac{3}{2})}\right)_{\sigma_1\sigma_2}(-i\,q) + \mathcal{O}(q^2). \end{aligned} \tag{15}$$

In this equation, $S_p = \frac{1}{2}$ is the spin of the proton and $S_{\Delta^+} = \frac{3}{2}$ is the spin of the Δ^+; u_2 and u_4 are the spin $1/2$ and spin $3/2$ solutions of the wave equation; $\vec{J}^{(\frac{1}{2})}$ and $\vec{J}^{(\frac{3}{2})}$ are the standard quantum mechanical spin operators for spin $1/2$ and $3/2$.

In units of $\mu_N = \frac{e}{2M}$ (M is the proton mass), the magnetic moments of the proton and the Δ^+ as defined by Eq. (15) are

$$\begin{aligned} \frac{\mu_p}{\mu_N} &= 1 + \lambda_p \\ &= 1 + \frac{4M(m+M)}{3m^2} + \frac{2M^2}{3m^2}(F_1 + F_2 + F_3 + F_5), \end{aligned} \tag{16}$$

$$\frac{\mu_{\Delta^+}}{\mu_N} = \frac{M}{m} + \left(-\frac{1}{2}F_1 + F_2\right). \tag{17}$$

When all the form factors are set to zero, $\mu_{\Delta^+} = \frac{e}{2m}$, so the g factor of the Δ^+ would be equal to $\frac{2}{3}$, which is expected for a minimally coupled particle of spin $3/2$ [57]. At the same time, partial-wave unitarity at high energy demands that the natural value of the g factor is equal to 2 for all spins [58,59]. Simple considerations based on the quark model suggest that the magnetic moment of the Δ^+ should be somewhat smaller than that of the proton, and imply that the actual value of the g factor is indeed somewhere between $2/3$ and 2.

In the minimally coupled case, the spin $1/2$ particle of our model has an anomalous magnetic moment from the second term in Eq. (16). The proton magnetic moment $\mu_p \simeq 2.79$ is well measured and acts as a constraint on the form factors through Eq. (16). Intriguingly, the actual value is close to that of the minimally coupled theory, so that $F_1 + F_2 + F_3 + F_5$ is approximately zero.

F_6 does not contribute to the magnetic moments because it is higher order in the soft photon momentum q. F_4 does not enter μ_{Δ^+} because $\gamma_\rho\psi^\rho = 0$ for the spin $3/2$ solution. F_4 does not appear in the proton magnetic moment either, as can be shown from the equations of motion.

In the limit of a degenerate mass for the proton and the Δ^+ (where in reality the mass gap is indeed small: $\frac{|m-M|}{M} \sim 0.3$), we can calculate the transition amplitude between a slowly moving proton and a Δ^+. We take the Δ^+ at rest: $p_1 = (m,0,0,0)$ and the proton momentum $p_2 = (\sqrt{M^2+q^2},0,0,q)$ and work in the degenerate $M \to m$ limit. We calculate $e\,\bar{u}_4(p_1,\sigma_1)\,\tilde{\Gamma}^\mu\,u_2(p_2,\sigma_2)\,A^{L/R}_\mu$. For a small q, the transition is $\mathcal{O}(q)$ and at the first order in q the result is

$$\begin{aligned} &e\bar{u}_4(p_1,\sigma_1)\tilde{\Gamma}^\mu u_2(p_2,\sigma_2)A^L_\mu \\ &\quad= 2\,M\,\mu_N\,G\,q\begin{pmatrix}\sqrt{3} & 0\\ 0 & 1\\ 0 & 0\\ 0 & 0\end{pmatrix}_{\sigma_1,\sigma_2} + \mathcal{O}(q^2), \\ &e\bar{u}_4(p_1,\sigma_1)\tilde{\Gamma}^\mu u_2(p_2,\sigma_2)A^R_\mu \\ &\quad= 2\,M\,\mu_N\,G\,q\begin{pmatrix}0 & 0\\ 0 & 0\\ -1 & 0\\ 0 & -\sqrt{3}\end{pmatrix}_{\sigma_1,\sigma_2} + \mathcal{O}(q^2), \end{aligned} \tag{18}$$

where $G = \frac{1}{12\sqrt{2}}(8 + 2\,F_1 + 8\,F_2 + F_5 - i\,F_4)$ determines the $M1$ transition amplitude between the proton and the Δ^+. The entries of the matrix are proportional to the appropriate Clebsch-Gordan coefficients. G is an important parameter and as we will see in the next section it makes the dominant contribution to the static magnetic polarizability in our model.

IV. COMPTON SCATTERING CROSS SECTION AND POLARIZABILITIES

At tree level, the Feynman diagrams for the proton Compton scattering are shown in Fig. 1. For the s and u channels, the propagator and the vertices were given in the previous section in Eqs. (2), (5), (6), (9), and (11).

For the pion exchange t-channel diagram, there is no contribution from the Δ^+, and we use the familiar Dirac spinor as the proton wave function. The relevant interaction Lagrangian is

$$\mathcal{L}_{\rm int} = i\, g_\pi\, \bar{u}\, \gamma^5\, u\, \pi^0 + \tfrac{1}{8}\, F_{\pi\gamma\gamma}\, \epsilon_{\mu\nu\rho\lambda}\, F^{\mu\nu}\, F^{\rho\lambda}\, \pi^0. \quad (19)$$

The incoming proton and photon have 4-momentum k_1 and k_2, and the outgoing proton and photon k_4 and k_3, respectively. With the above Feynman rules, the tree level amplitude is the sum of the four diagrams in Fig. 1:

$$\begin{aligned}\mathcal{A}_{\sigma_1,\sigma_4,\lambda_2,\lambda_3} = &\Big[(ie)^2\ \bar{u}_2(k_4,\sigma_4)\,\tilde{\Gamma}^\mu\,(-i)S(k_1-k_3)\,\tilde{\Gamma}^\nu\,u_2(k_1,\sigma_1) + (ie)^2\ \bar{u}_2(k_4,\sigma_4)\,\tilde{\Gamma}^\nu\,(-i)S(k_1+k_2)\,\tilde{\Gamma}^\mu\,u_2(k_1,\sigma_1)\\ &+\frac{ig_\pi\,F_{\pi\gamma\gamma}}{(k_1-k_4)^2-m_\pi^2}\,\bar{u}(k_4,\sigma_4)\,\gamma^5\,u(k_1,\sigma_1)\,\epsilon^{\mu\nu\sigma\rho}\,k_{2\sigma}\,k_{3\rho}\Big]\epsilon_\mu(k_2,\lambda_2)\,\epsilon^*_\nu(k_3,\lambda_3) \quad (20)\\ &+\frac{i\pi}{M}[\bar{u}_2(k_4,\sigma_4)\,\Gamma^\sigma\,\partial_\delta\,u_2(k_1,\sigma_1) - \partial_\delta\,\bar{u}_2(k_4,\sigma_4)\,\Gamma^\sigma u_2(k_1,\sigma_1)],\\ &\Big[(\alpha_B-\beta_B)\big(k_{3\sigma}\,\delta^\rho_\mu - k_3^\rho\,g_{\mu\sigma}\big)\big(k_{2\rho}\,\delta^\delta_\nu - k_2^\delta\,g_{\rho\nu}\big) - \frac{1}{2}\delta^\delta_\sigma\,\beta_B\big(k_3^\rho\,\delta^\gamma_\mu - k_3^\gamma\delta^\rho_\mu\big)\big(k_{2\rho}\,g_{\gamma\nu} - k_{2\gamma}\,g_{\rho\nu}\big)\Big]\epsilon_\mu(k_2,\lambda_2)\epsilon^*_\nu(k_3,\lambda_3).\end{aligned}$$

In addition to the diagrams in Fig. 1, strong interactions contribute through the pion one-loop diagrams as in Fig. 2. Above the pion-production threshold, the diagram (a) contributes to the imaginary part of the self-energy of the Δ^+ and determines the line shape of the resonance. In principle, the imaginary part depends on the center-of-mass momentum squared s, and all these diagrams should be taken into account at the one-loop order [47]. For our purposes, we make an estimate of this effect by setting the imaginary part of the Δ^+ mass m to the observed width at the resonance, i.e., we analytically extend the above matrix element by substituting m with $(m_0 - i\frac{\Gamma}{2}) \sim (1210 - 50i)$ MeV everywhere it appears in the matrix element. Despite modifications of both the vertex and the propagator, this procedure preserves the Ward identity from the analyticity of Eq. (4) in m.

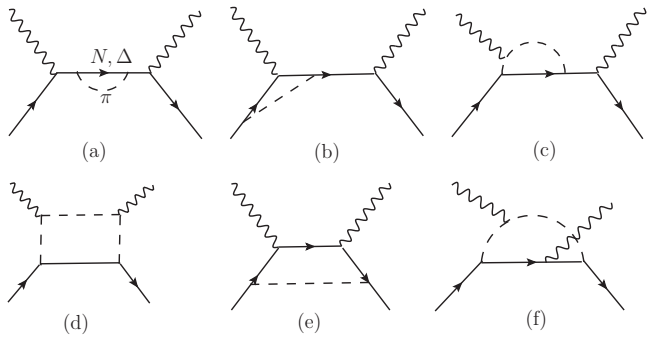

FIG. 2. The one-loop level pion corrections, at the second order in the pion-nucleon coupling: (a) is the self-energy correction; (b) and (c) are the pion vertex corrections. The first three diagrams are one-particle reducible, so that their contributions can be absorbed into the baryon propagator (a) and the electromagnetic vertices (b) and (c). These are especially important above the pion production threshold. The other three diagrams are one-particle irreducible (1PI) and therefore we model them by the effective four-point interaction of Eq. (13). There exist additional diagrams with the photon legs crossed.

It is verified that our result satisfies Low's theorem [18], namely that for the low-energy Compton scattering of spin 1/2 particles, the amplitudes expanded to the first order in the photon energy are completely determined by the mass, the electric charge, and the magnetic moment of the spin 1/2 particle. According to the theorem, in the laboratory frame with the photon incident energy ω, the amplitudes are

$$\begin{aligned}&\mathcal{A}_{\sigma_1,\sigma_4,\lambda_2,\lambda_3}\\ &= \frac{e^2}{M}\vec{\epsilon}_{\lambda_2}\cdot\vec{\epsilon}^{\,*}_{\lambda_3}\delta_{\sigma_1\sigma_2} - \frac{ie\omega}{M}\left(2\mu_p - \frac{e}{2M}\right)\big(\vec{\epsilon}^{\,*}_{\lambda_3}\times\vec{\epsilon}_{\lambda_2}\big)\cdot\vec{\sigma}_{\sigma_1\sigma_2}\\ &\quad + \frac{ie\mu_p}{\omega M}\big(\vec{\epsilon}_{\lambda_2}\cdot\vec{k}_3\big(\vec{\epsilon}^{\,*}_{\lambda_3}\times\vec{k}_3\big) - \vec{\epsilon}^{\,*}_{\lambda_3}\cdot\vec{k}_2\big(\vec{\epsilon}_{\lambda_2}\times\vec{k}_2\big)\big)\cdot\vec{\sigma}_{\sigma_1\sigma_2}\\ &\quad + \frac{2i\mu_p^2}{\omega}\big(\big(\vec{\epsilon}^{\,*}_{\lambda_3}\times\vec{k}_3\big)\times\big(\vec{\epsilon}_{\lambda_2}\times\vec{k}_2\big)\big)\cdot\vec{\sigma}_{\sigma_1\sigma_2} + O(\omega^2). \quad (21)\end{aligned}$$

The expansion of the cross section to the second order in the photon energy ω is exactly in the form of Eq. (12) with $\bar{\alpha} \pm \bar{\beta}$:

$$\begin{aligned}\bar{\alpha}+\bar{\beta} \sim\ & -0.860 - 0.556F_1 - 1.789F_2 - 0.240F_5\\ & - 0.069F_1^2 - 0.961F_2^2 - 0.015F_4^2 - 0.020F_5^2\\ & - 0.536F_1F_2 - 0.023F_1F_3 - 0.085F_1F_5\\ & + 0.009F_2F_3 - 0.234F_2F_5 - 0.007F_3F_5\\ & + \alpha_B + \beta_B\ (10^{-4}fm^3), \quad (22)\\ \bar{\alpha}-\bar{\beta} \sim\ & 1.894 + 1.284F_1 + 2.602F_2 + 0.202F_3 + 0.650F_5\\ & + 0.146F_1^2 + 1.339F_2^2 + 0.028F_3^2 + 0.023F_4^2\\ & + 0.064F_5^2 + 0.728F_1F_2 + 0.069F_1F_3\\ & + 0.177F_1F_5 + 0.101F_2F_3 + 0.447F_2F_5\\ & + 0.067F_3F_5 + \alpha_B - \beta_B\ (10^{-4}fm^3),\end{aligned}$$

where α_B and β_B are the bare polarizabilities defined in Eq. (13).

To conclude, we note that the influence of the parameters $F_{1..6}$ at the second order in energy is degenerate: There are only two polarizabilities which enter at the second order in the energy of the photon. At higher orders in energy this degeneracy is broken, and one can in principle relate the appropriate combinations of $F_{1..6}$ to the spin polarizabilities, conventionally defined as the coefficients of the third order in the energy.

V. THE AMPLITUDES NEAR THE Δ^+ POLE

The Δ^+ and the proton are almost degenerate in mass:

$$m = M(1 + x - iy), \tag{23}$$

where $x \sim 0.3$ and $y \sim 0.05 \sim \frac{1}{2}x^2$. In addition, around the Δ^+ resonance, the photon momentum $\frac{q}{M}$ is of the same order as x, thus we can approximate the amplitudes to the lowest nontrivial order in $\frac{q}{M}$, x and y.

First, at the Δ^+ pole position, the contribution to the pole mainly comes from the first term in the propagator in the s channel where the momentum in the propagator is $k_1 + k_2$. In this case, the denominator contributing to the pole is $(k_1 + k_2)^2 - m^2 = (E_{\rm CM} - m)(E_{\rm CM} + m)$. We multiply the amplitudes by $(E_{\rm CM} - m)$ and then expand it with respect to $\frac{q}{M}$, x, and y. We define $\frac{q}{M} = r_1 x$ and $y = r_2 x^2$. Around the peak, $r_1 \sim 1$ and $r_2 \sim 0.5$. Then we can expand the amplitudes, premultiplied by $(E_{\rm CM} - m)$, with respect to x, and finally set $r_1 = 1$ (at the peak) and $r_2 = \frac{y}{x^2}$. In the center-of-mass frame, we rotate the proton wave function to make it polarized along its direction of movement; that is, for a proton moving in the direction θ with respect to the z axis,

$$\begin{aligned}
&\tilde{u}_2\left(p, \frac{1}{2}\right) \\
&\quad = \cos\left(\frac{\theta}{2}\right) u_2\left(p, \frac{1}{2}\right) + \sin\left(\frac{\theta}{2}\right) u_2\left(p, -\frac{1}{2}\right), \\
&\tilde{u}_2\left(p, -\frac{1}{2}\right) \\
&\quad = -\sin\left(\frac{\theta}{2}\right) u_2\left(p, \frac{1}{2}\right) + \cos\left(\frac{\theta}{2}\right) u_2\left(p, -\frac{1}{2}\right).
\end{aligned} \tag{24}$$

Then the approximate amplitudes are

$$\begin{aligned}
\mathcal{A}_{ppRR} &= \frac{(2ir_2 + 1 - 6|G|^2)x^2 \cos^3\frac{\theta}{2}}{2(E_{\rm CM} - m)}, \\
\mathcal{A}_{ppRL} &= \frac{(-2ir_2 - 1 - 6|G|^2)x^2 \cos\frac{\theta}{2}\sin^2\frac{\theta}{2}}{2(E_{\rm CM} - m)}, \\
\mathcal{A}_{ppLR} &= \frac{(-2ir_2 - 1 - 6|G|^2)x^2 \cos\frac{\theta}{2}\sin^2\frac{\theta}{2}}{2(E_{\rm CM} - m)}, \\
\mathcal{A}_{ppLL} &= \frac{(2ir_2 + 1 + 6|G|^2 + (2ir_2 + 1 - 18|G|^2)\cos\theta)x^2 \cos\frac{\theta}{2}}{4(E_{\rm CM} - m)}, \\
\mathcal{A}_{pmRR} &= \frac{(2ir_2 + 1 - 6|G|^2)x^2 \cos^2\frac{\theta}{2}\sin\frac{\theta}{2}}{2(E_{\rm CM} - m)}, \\
\mathcal{A}_{pmRL} &= \frac{(-2ir_2 - 1 - 6|G|^2)x^2 \sin^3\frac{\theta}{2}}{2(E_{\rm CM} - m)}, \\
\mathcal{A}_{pmLR} &= \frac{(-2ir_2 - 1 + 2|G|^2 + (2ir_2 + 1 + 6|G|^2)\cos\theta)x^2 \sin\frac{\theta}{2}}{4(E_{\rm CM} - m)}, \\
\mathcal{A}_{pmLL} &= \frac{(2ir_2 + 1 - 6|G|^2)x^2 \cos^2\frac{\theta}{2}\sin\frac{\theta}{2}}{2(E_{\rm CM} - m)}.
\end{aligned} \tag{25}$$

In the above expressions, $x = \frac{{\rm Re}(m) - M}{M}$, $r_2 = \frac{y}{x^2} = -\frac{{\rm Im}(m)}{Mx^2}$. G is the combination of the form factors which describes the $\gamma N \Delta^+$ transition amplitude as described in the previous section in Eq. (18). For the subscript of the amplitudes, the first(second) $p(m)$ stands for the final(initial) proton polarization and the first(second) $L(R)$ for the final(initial) photon polarization. Here only eight of the 16 amplitudes are given, because the other eight are related by parity:

$$\begin{aligned}
\mathcal{A}_{mmRR} &= \mathcal{A}_{ppLL}, \quad \mathcal{A}_{mpRR} = -\mathcal{A}_{pmLL}, \\
\mathcal{A}_{mmRL} &= \mathcal{A}_{ppLR}, \quad \mathcal{A}_{mpRL} = -\mathcal{A}_{pmLR}, \\
\mathcal{A}_{mmLR} &= \mathcal{A}_{ppRL}, \quad \mathcal{A}_{mpLR} = -\mathcal{A}_{pmRL}, \\
\mathcal{A}_{mmLL} &= \mathcal{A}_{ppRR}, \quad \mathcal{A}_{mpLL} = -\mathcal{A}_{pmRR}.
\end{aligned} \tag{26}$$

In the same limit, the magnetic polarizability has an approximation:

$$\bar{\beta} = -\frac{4\alpha|G|^2}{xM^3} + \beta_B. \tag{27}$$

This implies that the magnetic polarizability is directly related to the proton-Δ (magnetic) transition [60,61].

VI. FITTING DATA

We fit the model to the 714 proton Compton scattering data points from eight experiments [1–3,5,7–10]. Only the data points with the photon incident energy smaller than 455 MeV

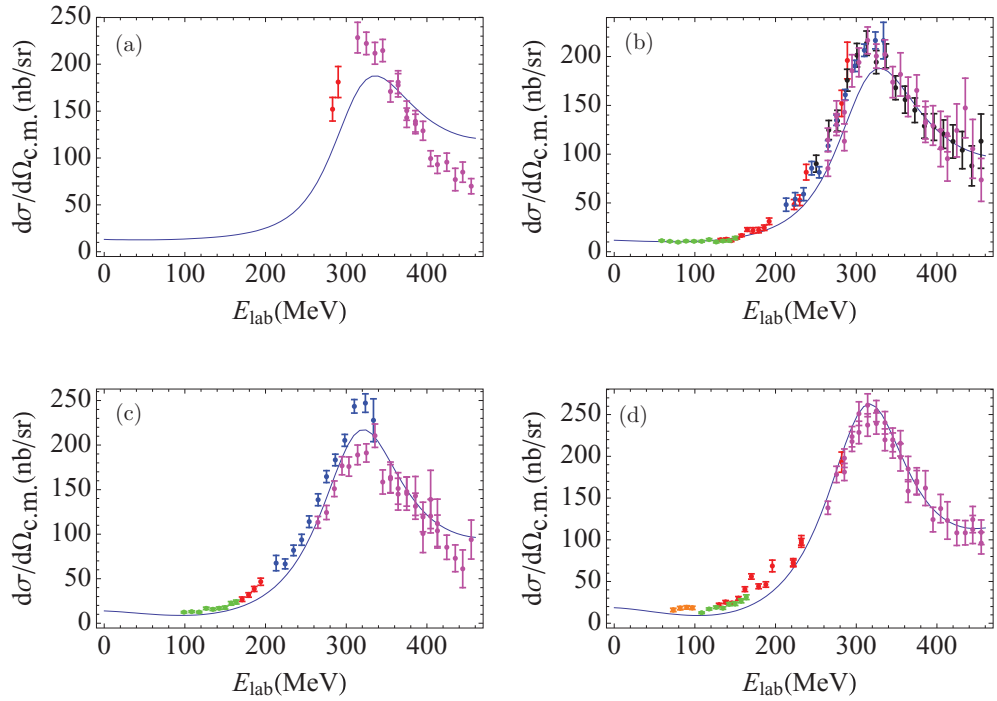

FIG. 3. (Color online) Fixed c.m. angle cross section and the data points, where the parameters from the fitting to all the 714 data points are used for the theoretical cross-section curve. (a) c.m. frame cross section at $\theta_{\text{c.m.}} = 70^\circ$; (b) c.m. frame cross section at $\theta_{\text{c.m.}} = 90^\circ$; (c) c.m. frame cross section at $\theta_{\text{c.m.}} = 115^\circ$; (d) c.m. frame cross section at $\theta_{\text{c.m.}} = 140^\circ$. The x axis is the lab frame photon energy and the y axis is the c.m. frame differential cross section in units of nanobarn. For [1–3,5,7–10], we use the following colors: cyan, darker pink, black, orange, red, blue, green, and magenta, respectively. The angles of the data points included in this plot may differ from the nominal by at most 3°.

are used, i.e., in the first resonance region. In principle, one can also compare the model predictions with the polarized measurements, where some data are available [6,16]. On the theoretical side, lattice QCD may perhaps be used to measure the necessary observables [62].

We set $F_4 = 0$ in our fitting for several reasons. First, F_4 does not appear in the expressions of the proton and the Δ^+ magnetic moments Eqs. (16) and (17). Second, in all the fits we attempted, the best fit value of F_4 was near exactly zero, and statistically consistent with zero.

The parameters we use to fit are F_1, $\mu \equiv \frac{\mu_\Delta^+}{\mu_N} = \frac{M}{m} + F_2 - \frac{1}{2}F_1$, $G = \frac{1}{12\sqrt{2}}(8 + 2F_1 + 8F_2 + F_5)$, F_6 and the bare polarizabilities α_B and β_B in Eq. (13). F_3 is constrained by the proton magnetic moment; see Eq. (16).

We minimize $\chi^2 = \sum_{i=1}^{714} \frac{((\frac{d\sigma}{d\Omega})_i^{\text{calc}} - (\frac{d\sigma}{d\Omega})_i^{\text{data}})^2}{\sigma_{(\text{stat})i}^2 + \sigma_{(\text{syst})i}^2}$. We did not attempt to rescale the data of each experiment within its own systematical uncertainty to see if it would lead to better consistency between data sets as it was done in Ref. [63]. The optimal set of parameters is found to be $F_1 = -27.5$, $\mu = 14.2$, $G = 1.81$, $F_6 = 12.9$, $\alpha_B = 7.5$, $\beta_B = -8.2$ with $\chi^2 \sim 6.3 \times 10^3$, see Table I.

TABLE I. Our best-fit parameter values and confidence levels in the resonance region. The 95% confidence levels are given in the table.

	F_1	G	μ	F_6	α_B	β_B
Whole data	−27.5	1.81	14.2	12.9	7.5	−8.2
95% C.L.	2.8	0.05	1.1	1.7	2.2	1.6
MAMI data	−27.7	1.83	14.2	14.8	2.1	−8.1
95% C.L.	1.4	0.03	0.7	1.5	1.5	1.1

On average the data points are 3σ away from the fit values. The Δ^+ resonance region is fitted well, while the low-energy cross section deviates greatly from the data points. In fact, the 68 data points with the incident photon energy smaller than 140 MeV out of the total 714 data points contribute nearly a third to the total χ^2. Our fit cannot take care of the low energy ($\lesssim$140 MeV) data points and the high energy ($\gtrsim$200 MeV) data points simultaneously. When finding a good fit in the resonance region, where most data points used lie, the predicted cross section at low energy cannot account for the large asymmetry of the cross-section data at forward and backward angles. Our fit cross sections at low energies are much higher than the data at forward angles and lower at backward angles. Because the polarizabilities are extracted according to a low-energy expansion of the cross section in Eq. (12), it is expected that $\bar{\alpha} + \bar{\beta}$, calculated using Eq. (22) is smaller than the experimental value, and $\bar{\alpha} - \bar{\beta}$ larger than the experimental value.

We plot the center-of-mass (c.m.) frame cross section using the above fit parameters, together with the data points, in Figs. 3 and 4.

The challenge is clearly that the low-energy part and the Δ^+ resonance range data points are difficult to fit well at the same time. The form factors (and thus the parameters μ

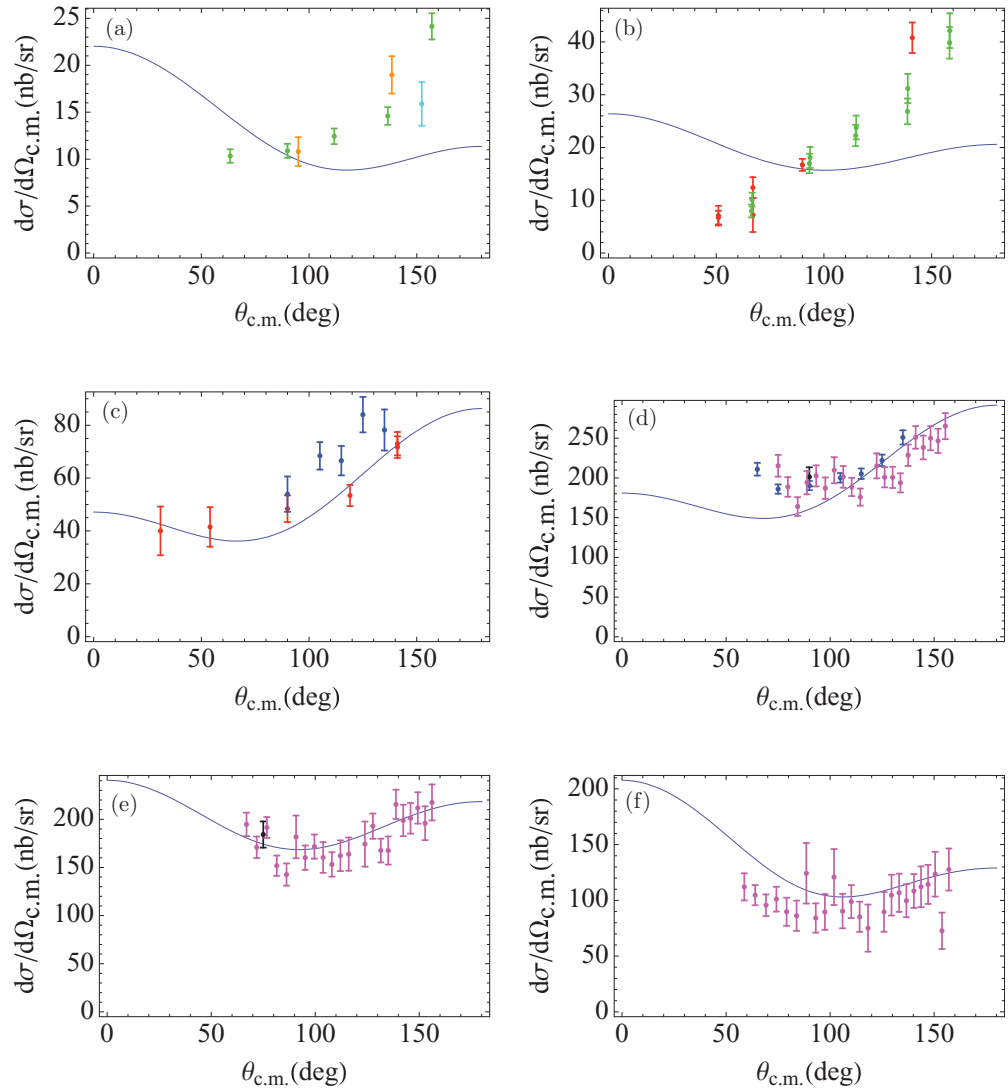

FIG. 4. (Color online) The c.m. cross section at fixed photon incident energy and the data points, where the parameters from the fitting to all the 714 data points are used for the theoretical cross-section curve. (a) c.m. frame cross section at $E_{\text{lab}} = 90$ Mev; (b) c.m. frame cross section at $E_{\text{lab}} = 160$ Mev; (c) c.m. frame cross section at $E_{\text{lab}} = 225$ Mev; (d) c.m. frame cross section at $E_{\text{lab}} = 300$ Mev; (e) c.m. frame cross section at $E_{\text{lab}} = 355$ Mev; (f) c.m. frame cross section at $E_{\text{lab}} = 425$ Mev. The x axis is the c.m. frame scattering angle and the y axis is the c.m. frame differential cross section in units of nanobarn. Labels are the same as in Fig. 3. The quoted photon energy of the data points included in the plots may differ from the nominal values by at most 4 MeV.

and G) are generally functions of k^2 where k is the photon momentum. For real Compton scattering, k^2 is always zero, so the form factors should be constants. However, in the case of the bare polarizabilities it is possible that they vary with energy and/or scattering angle [32], which would make fitting with constant bare polarizabilities unsuccessful. In fact, the dynamical behavior of the polarizabilities, including the nonanalyticity near the pion threshold can only be successfully accounted for by including the pion loop correction within the chiral perturbation theory approach [49–51,64,65]

The strategy we propose to minimize the impact of the dynamical behavior of the polarizabilities is as follows. First, we fit only the peak range data points and fix the form factors (including μ and G) from this fitting. Then we fit the low-energy data points varying only the bare polarizabilities. For the peak range, we use only the MAMI(2001) experiment [10], which contains 436 data points with photon incident energy ranging from 260 MeV to 455 MeV. A good fit is achieved at $F_1 = -27.7$, $G = 1.83$, $\mu = 14.2$, $F_6 = 14.8$, $\alpha_B = 2.1$, $\beta_B = -8.1$ with $\chi^2 \sim 830$, see Table I. Notice that F_1, F_6, μ, and G have not changed much from the complete fit of all data points, yet χ^2 per data point is much smaller. This may be indicative of the fact that the experimental data prior to these latest and more precise measurements may not be consistent with each other. In the past, one of the strategies for dealing with this (see [63]) was to allow rescaling the cross-section data for each experiment within the systematical uncertainty which tends to be large.

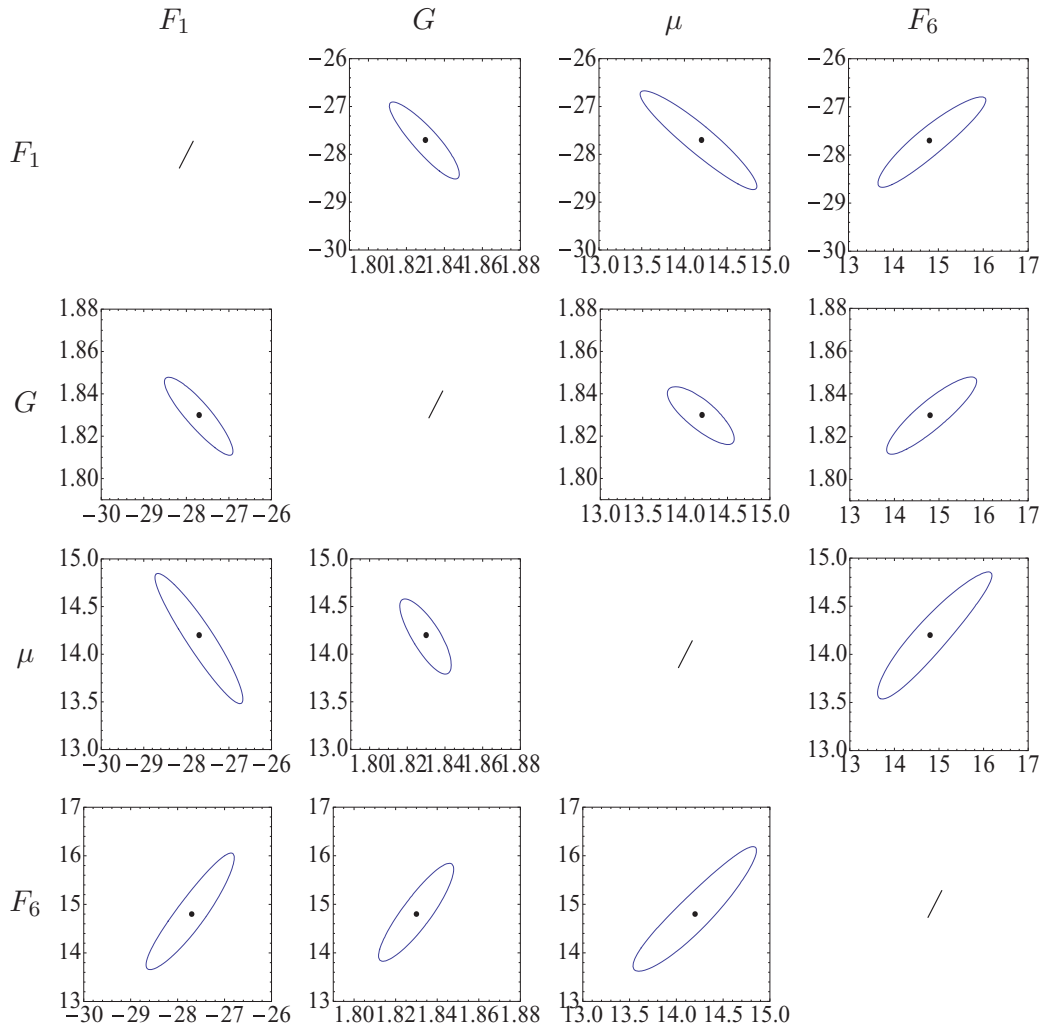

FIG. 5. (Color online) Projections of the six-dimensional 95% confidence region into planes spanned by several pairs of the parameters. The plots in each column share the same x-axis parameter as indicated at the top of each column. The plots in each row share the same y-axis parameter as indicated at the left of each row. The range for F_1 is (−30,−26); G: (1.79,1.88); μ: (13,15); F_6: (13,17).

Qualitatively, we found that changes in the μ_{Δ^+} affect the predicted cross-section asymmetrically: Lower values of the magnetic moment do not drastically change the prediction, but higher values greatly enhance the cross section, both on and off the resonance. Therefore we exclude any values of the Δ^+ magnetic moment μ_{Δ^+} larger than about 14.2. This should be compared to the value extracted by MAMI [66] at $2.7^{+1.0}_{-1.3}(\text{stat}) \pm 1.5(\text{syst}) \pm 3(\text{theor})$, but notice that the error is dominated by theoretical model uncertainty. Our upper bound is also consistent with expectations from a naive quark model and some model calculations [67,70].

The inclusion of the sigma channel and/or variation of the mass and width of the sigma meson do not appreciably alter the goodness-of-fit or the values of the optimal parameters.

In Fig. 5, we give the contour plots of χ^2 with respect to several pairs of parameters for this fit. It is seen that G is very strictly constrained.

We then fix these values for F_1, F_6, μ, and G and fit the low-energy data points, varying only α_B and β_B. We take 68 data points with photon incident energy below 140 MeV and obtain the best fit values of $\alpha_B = -4.6$ and $\beta_B = 17.9$ with $\chi^2 \sim 194$. See Figs. 6 and 7. For these optimal parameter values, the total polarizabilities, $\bar{\alpha} + \bar{\beta} = 11.3 \pm 0.9 \pm 2.3(95\%\,\text{C.L.})$ and $\bar{\alpha} - \bar{\beta} = 7.8 \pm 3.3 \pm 2.0(95\%\,\text{C.L.})$, are much closer to values extracted (from the same data) previously. The first error is determined from the high energy fit, by investigating how the contributions of F_1, G, and μ to the polarizabilities vary in the three-dimensional 95% confidence region spanned by these three parameters. The second quoted error is statistical.

The important conclusion which can be inferred from Table II (the second line) is that the extraction of the backward polarizability, $\bar{\alpha} - \bar{\beta}$, is influenced by the uncertainties in the model parameters which are degenerate at the second order in the photon energy such as F_1, F_6, and μ_Δ (for fixed G and μ_N). Stated in more familiar language, the influence of the unknown spin polarizabilities makes itself felt through the variation of the model prediction in the 80- to 140-MeV region. This would not be the case if data could be taken at arbitrarily low energy

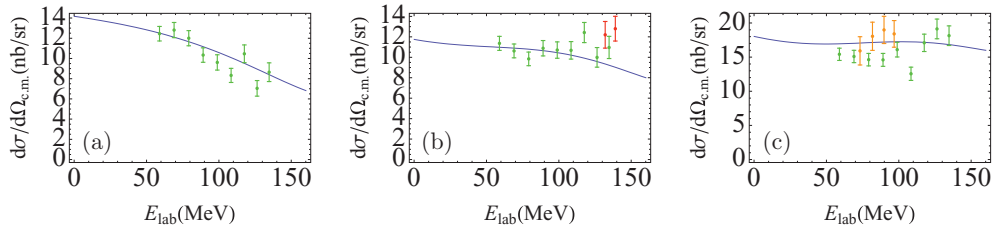

FIG. 6. (Color online) Fixed c.m. angle cross section and the data points with photon incident energy below 140 MeV, for the fit parameters of the low-energy data points. (a) c.m. frame cross section at $\theta_{\text{c.m.}} = 63^\circ$; (b) c.m. frame cross section at $\theta_{\text{c.m.}} = 90^\circ$; (c) c.m. frame cross section at $\theta_{\text{c.m.}} = 137^\circ$. The x axis is the laboratory frame photon energy and the y axis is the c.m. frame differential cross section in units of nanobarn. The angles of the data points included may differ from the nominal by at most 2.5°. The labels are the same as in Fig. 3.

or if the radius of convergence of the power series in energy were greater.

VII. DISCUSSION

At the dawn of the particle and nuclear physics, there had been considerable doubt as to the right relativistic equation to describe the proton. Some of this doubt was because of the fact that the Dirac equation in its original form could not describe or explain the large anomalous magnetic moment of the proton. Eventually, the Dirac Lagrangian with the addition of an effective term corresponding to the anomalous magnetic moment became well accepted. Nevertheless, an alternative to the Dirac equation to describe the proton had been proposed by Bhabha: Long before the quark model he suggested that his three-mass-state relativistic spin $3/2$ equation could be used to describe the proton. In his opinion, the proton in the high-energy regime could exhibit its hidden spin $3/2$ nature. We now know this to be more or less correct, because there are indeed three spin $1/2$ quarks inside the proton. Unfortunately, in his equation the ratio of the mass of the spin $1/2$ and spin $3/2$ components was rigidly fixed to 3, and there was a second spin $1/2$ component which has incorrect pole structure indicating that it is a ghost. In the equation of Ranada and Sierra [52] the second, unphysical, spin $1/2$ component is projected out and the resulting equation with some additional restriction on the mass ratio has unitary pole structure and completely transverse physical modes [53].

The model of electromagnetic properties of the proton which we developed on this basis in Secs. II and III is of general nature and has applicability to many processes in the few-hundred MeV energy range, i.e., whenever there is an off-shell proton in some intermediate state. Other than proton Compton scattering it can be applied, for example, to calculations of two-photon exchange in elastic electron scattering. The predictions of the model are different from the standard approach of treating the proton as a Dirac particle with anomalous magnetic moment, and the Δ^+ as a Rarita-Schwinger particle. In particular, at higher energies, there is a destructive interference between the contributions of the virtual proton and the Δ^+.

Our model incorporates both minimal and nonminimal couplings. The former takes into account that the Δ^+ is charged, a fact which presents difficulties in the standard approach because of the possibility of unphysical poles in the dressed propagator. In our model, it is assured that such unphysical poles do not appear.

The existence of the nonminimal couplings necessitates the introduction of a small number of free parameters. Most of these parameters have a clear physical interpretation, namely as the proton and the Δ^+ magnetic moments, as well as the strength of the $N\Delta$ magnetic transition ($M1$) and the two bare polarizabilities. The contributions of the parameters which are degenerate at the second order in the photon energy (F_1, F_6, and μ_Δ) are disentangled at the third order, where the coefficients are usually interpreted as the spin polarizabilities. This should be contrasted with the standard approach [64] where there is just one parameter to describe the strength of the $M1$ transition. Fortunately, very precise data which is sufficient to determine the entire set of spin polarizabilities will soon become available. One can expect that the quantitative and the qualitative differences between the predictions of

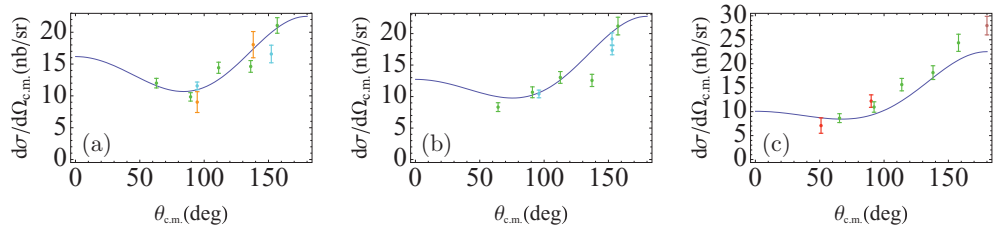

FIG. 7. (Color online) The fit cross section and the data points with photon incident energy below 140 MeV, for the fit parameters of the low-energy data points. (a) c.m. frame cross section at $E_{\text{lab}} = 80$ MeV; (b) c.m. frame cross section at $E_{\text{lab}} = 109$ MeV; (c) c.m. frame cross section at $E_{\text{lab}} = 133$ MeV. The x axis is the c.m. frame scattering angle and the y axis is the c.m. frame differential cross section in units of nanobarn. The incident energy of the data points included in this plot may differ from the nominal by at most 2.5 MeV. The labels are the same as in Fig. 3.

TABLE II. Our best-fit parameter values for polarizabilities and confidence regions inferred from the low-energy fit. The 95% confidence levels are given in the table.

	Value	95% C.L. model error from high-energy parameters	95% C.L. stat error
$\bar{\alpha}+\bar{\beta}$	11.3	±0.9	±2.3
$\bar{\alpha}-\bar{\beta}$	7.8	±3.3	±2.0

different models in the energy range below the peak will then become more pronounced, and that it will be necessary to introduce additional terms in the effective Lagrangian in the standard approach as well. Our approach already incorporates the necessary flexibility to fit the spin polarizabilities to data.

Although we have been able to extract a value for the Δ^+ magnetic moment, we cannot have a very high confidence in this value because the proton Compton scattering does not probe the $\gamma\Delta^+\Delta^+$ vertex directly. It is possible to extract this because the form factors have definite properties under the Lorentz transformations, so that the same set of parameters which affects the Compton process also determines the magnetic moment of the Δ^+. The more reliable path towards determining the Δ^+ magnetic moment would be to extend the model to include the pions and thus cover the case of pion photoproduction $\gamma N \to \pi N$ and $\gamma N \to \pi N\gamma$. An extension of the model to include the interaction with the pion, within the framework of chiral perturbation theory, will be published in an upcoming paper.

ACKNOWLEDGMENTS

The authors would like to thank G. Georgiou and J. D. Vergados for their valuable comments. This research project has been supported in parts by the Jiangsu Ministry of Science and Technology under Contract No. BK20131264 and by the Swedish Research Links programme of the Swedish Research Council (Vetenskapsradets generella villkor) under Contract No. 348-2008-6049. We also acknowledge the 985 Grants from the Ministry of Education, and the Priority Academic Program Development for Jiangsu Higher Education Institutions (PAPD).

APPENDIX: $\Delta^+ \to N + \gamma$ DECAY WIDTH

Aside from the proton Compton scattering, another process can be readily accounted for in this unified $N-\Delta^+$ electromagnetic model, that is, the decay $\Delta^+ \to N+\gamma$. The Feynman rules for this diagram were given in Sec. II.

We label the momentum and polarization of the Δ^+ as k_1, σ_1, the produced photon k_2,λ_2 and the proton k_3,σ_3, the matrix element is

$$\mathcal{A}_{\sigma_1,\lambda_2,\sigma_3} = e\ \bar{u}_2(k_3,\sigma_3)\,\tilde{\Gamma}^\mu\,u_4(k_1,\sigma_1)\,\epsilon^*_\mu(k_2,\lambda_2). \tag{A1}$$

It is of interest to find the decay width $\Gamma_{3/2}$ and $\Gamma_{1/2}$ for the final state helicity $\frac{3}{2}$ and $\frac{1}{2}$, respectively. Evaluating this amplitude, we obtain after substituting the values of m, M,

$$\begin{aligned}
\Gamma_{3/2} &= 0.0047F_1^2 + 0.056F_2^2 + 0.001F_4^2 + 0.001F_5^2 \\
&\quad + 0.032F_1F_2 + 0.004F_1F_5 + 0.0139F_2F_5 + 0.032F_1 \\
&\quad + 0.1113F_2 + 0.0139F_5 + 0.0557\ \text{MeV}, \\
\Gamma_{1/2} &= 0.0004F_1^2 + 0.0120F_2^2 + 0.0002F_4^2 + 0.0002F_5^2 \\
&\quad + 0.0002F_6^2 + 0.0058F_1F_2 + 0.0005F_1F_5 \\
&\quad - 0.0006F_1F_6 + 0.0037F_2F_5 - 0.0039F_2F_6 \\
&\quad - 0.0004F_5F_6 + 0.0043F_1 + 0.0293F_2 + 0.0027F_5 \\
&\quad - 0.0028F_6 + 0.0108\ \text{MeV}.
\end{aligned} \tag{A2}$$

If, on the other hand, we let $m = M(1+x)$ then in the limit of small x we find

$$\begin{aligned}
\Gamma_{3/2} &\sim 3\alpha M x^3 |G|^2, \\
\Gamma_{1/2} &\sim \alpha M x^3 |G|^2.
\end{aligned} \tag{A3}$$

Experimentally, the $\Delta^+ \to p+\gamma$ decay amplitudes can be extracted from the Δ^+ peak of the proton Compton scattering [8]. For the optimal fit parameters for the MAMI data we obtained in Sec. VI we calculate $\Gamma_{3/2} = 0.43$ MeV and $\Gamma_{1/2} = 0.11$ MeV, close to the values quoted in [8,71–74]: $\Gamma_{3/2} = 0.49 - 0.56$ MeV and $\Gamma_{1/2} = 0.13 - 0.15$ MeV.

[1] P. S. Baranov, G. M. Buinov, V. G. Godin, V. A. Kuznetsova, V. A. Petrunkin, L. S. Tatarinskaya, V. S. Shirchenko, L. N. Shtarkov *et al.*, Pisma Zh. Eksp. Teor. Fiz. **19**, 777 (1974).

[2] A. Zieger, R. Van de Vyver, D. Christmann, A. De Graeve, C. Van den Abeele, and B. Ziegler, Phys. Lett. B **278**, 34 (1992).

[3] A. Hunger, J. Peise, A. Robbiano, J. Ahrens, I. Anthony, H. J. Arends, R. Beck, G. P. Capitani *et al.*, Nucl. Phys. A **620**, 385 (1997).

[4] F. J. Federspiel, R. A. Eisenstein, M. A. Lucas, B. E. MacGibbon, K. Mellendorf, A. M. Nathan, A. O'Neill, and D. P. Wells, Phys. Rev. Lett. **67**, 1511 (1991).

[5] B. E. MacGibbon, G. Garino, M. A. Lucas, A. M. Nathan, G. Feldman, and B. Dolbilkin, Phys. Rev. C **52**, 2097 (1995).

[6] Y. Wada, S. Kato, T. Miyachi, K. Sugano, K. Toshioka, K. Ukai, T. Ishii, K. Egawa *et al.*, Nuovo Cimento A **63**, 57 (1981).

[7] E. L. Hallin, D. Amendt, J. C. Bergstrom, H. S. Caplan, R. Igarashi, D. M. Skopik, E. C. Booth, D. D. Carpini *et al.*, Phys. Rev. C **48**, 1497 (1993).

[8] G. Blanpied, M. Blecher, A. Caracappa, R. Deininger, C. Djalali, G. Giordano, K. Hicks, S. Hoblit *et al.*, Phys. Rev. C **64**, 025203 (2001).

[9] V. Olmos de Leon, F. Wissmann, P. Achenbach, J. Ahrens, H. J. Arends, R. Beck, P. D. Harty, V. Hejny *et al.*, Eur. Phys. J. A **10**, 207 (2001).

[10] S. Wolf, V. Lisin, R. Kondratiev, A. M. Massone, G. Galler, J. Ahrens, H. J. Arends, R. Beck *et al.*, Eur. Phys. J. A **12**, 231 (2001).

[11] A. Danagoulian *et al.* (Hall A. Collaboration), Phys. Rev. Lett. **98**, 152001 (2007).

[12] C. E. Hyde and K. de Jager, Ann. Rev. Nucl. Part. Sci. **54**, 217 (2004).

[13] M. Schumacher, Prog. Part. Nucl. Phys. **55**, 567 (2005).
[14] N. Krupina and V. Pascalutsa, Phys. Rev. Lett. **110**, 262001 (2013).
[15] F. V. Adamian, A. Y. Bunyatyan, G. S. Frangulian, P. I. Galumian, V. G. Grabsky, A. V. Airapetian, G. G. Akopian, V. K. Oktanian *et al*., J. Phys. G **19**, L139 (1993).
[16] G. Blanpied *et al*. (LEGS Collaboration), Phys. Rev. Lett. **76**, 1023 (1996).
[17] J. L. Powell, Phys. Rev. **75**, 32 (1949).
[18] F. E. Low, Phys. Rev. **96**, 1428 (1954).
[19] M. Gell-Mann and M. L. Goldberger, Phys. Rev. **96**, 1433 (1954).
[20] A. C. Hearn and E. Leader, Phys. Rev. **126**, 789 (1962).
[21] W. Pfeil, H. Rollnik, and S. Stankowski, Nucl. Phys. B **73**, 166 (1974).
[22] A. I. L'vov, Sov. J. Nucl. Phys. **34**, 597 (1981); Yad. Fiz. **34**, 1075 (1981).
[23] D. Drechsel, M. Gorchtein, B. Pasquini, and M. Vanderhaeghen, Phys. Rev. C **61**, 015204 (1999).
[24] A. I. L'vov, V. A. Petrunkin, and S. A. Startsev, Yad. Fiz. **29**, 1265 (1979).
[25] I. Guiasu, C. Pomponiu, and E. Radescu, Annals Phys. **114**, 296 (1978).
[26] A. M. Baldin, Nucl. Phys. **18**, 310 (1960).
[27] B. Pasquini, D. Drechsel, and M. Vanderhaeghen, Phys. Rev. C **76**, 015203 (2007).
[28] A. I. L'vov, Int. J. Mod. Phys. A **8**, 5267 (1993).
[29] A. I. L'vov, V. A. Petrun'kin, and M. Schumacher, Phys. Rev. C **55**, 359 (1997).
[30] V. A. Petrunkin, Fiz. Elem. Chastits At. Yadra **12**, 692 (1981).
[31] A. I. L'vov, Phys. Lett. B **304**, 29 (1993).
[32] M. Schumacher and M. D. Scadron, arXiv:1301.1567.
[33] E. E. Jenkins and A. V. Manohar, Phys. Lett. B **259**, 353 (1991); A. F. Falk, Nucl. Phys. B **378**, 79 (1992).
[34] S. Kondratyuk and O. Scholten, Phys. Rev. C **64**, 024005 (2001).
[35] G. Dattoli, G. Matone, and D. Prosperi, Lett. Nuovo Cimento **19**, 601 (1977).
[36] T. Feuster and U. Mosel, Phys. Rev. C **59**, 460 (1999).
[37] S. Weinberg, Physica A **96**, 327 (1979).
[38] J. Gasser and H. Leutwyler, Annals Phys. **158**, 142 (1984).
[39] R. D. Peccei, Phys. Rev. **176**, 1812 (1968).
[40] R. D. Peccei, Phys. Rev. **181**, 1902 (1969).
[41] M. Benmerrouche, R. M. Davidson, and N. C. Mukhopadhyay, Phys. Rev. C **39**, 2339 (1989).
[42] V. Pascalutsa and O. Scholten, Nucl. Phys. A **591**, 658 (1995).
[43] O. Scholten, A. Y. Korchin, V. Pascalutsa, and D. Van Neck, Phys. Lett. B **384**, 13 (1996).
[44] V. Lensky and V. Pascalutsa, PoS EFT **09**, 033 (2009).
[45] V. Pascalutsa and R. Timmermans, Phys. Rev. C **60**, 042201(R) (1999).
[46] V. Lensky and V. Pascalutsa, Eur. Phys. J. C **65**, 195 (2010).
[47] J. A. McGovern, D. R. Phillips, and H. W. Griesshammer, Eur. Phys. J. A **49**, 12 (2013).
[48] T. R. Hemmert, B. R. Holstein, and J. Kambor, Phys. Rev. D **55**, 5598 (1997).
[49] D. R. Phillips, J. A. McGovern, and H. W. Griesshammer, Eur. Phys. J. A **49**, 1 (2013).
[50] H. W. Griesshammer, J. A. McGovern, D. R. Phillips, and G. Feldman, Prog. Part. Nucl. Phys. **67**, 841 (2012).
[51] V. Lensky, J. A. McGovern, D. R. Phillips, and V. Pascalutsa, Phys. Rev. C **86**, 048201 (2012).
[52] A. F. Rannada and G. Sierra, Phys. Rev. D **22**, 2416 (1980).
[53] K. G. Savvidy, arXiv:1111.5076.
[54] G. Chen and K. G. Savvidy, Eur. Phys. J. C **72**, 1952 (2012).
[55] A. Ilyichev, S. Lukashevich, and N. Maksimenko, arXiv:cond-mat/0611327.
[56] D. Babusci, G. Giordano, A. I. L'vov, G. Matone, and A. M. Nathan, Phys. Rev. C **58**, 1013 (1998).
[57] F. J. Belinfante, Phys. Rev. **92**, 997 (1953).
[58] C. Alexandrou *et al*. Nucl. Phys. A **825**, 115 (2009).
[59] C. Lorce, Phys. Rev. D **79**, 113011 (2009).
[60] R. Weiner and W. Weise, Phys. Lett. B **159**, 85 (1985).
[61] N. N. Scoccola and W. Weise, Nucl. Phys. A **517**, 495 (1990).
[62] J. D. Ashley, D. B. Leinweber, A. W. Thomas, and R. D. Young, Eur. Phys. J. A **19**, 9 (2004).
[63] P. S. Baranov, A. I. L'vov, V. A. Petrun'kin, and L. N. Shtarkov, in 9th International Seminar on Electromagnetic Interactions of Nuclei at Low and Medium Energies, September 2000, Moscow, Russia.
[64] V. Pascalutsa, M. Vanderhaeghen, and S. N. Yang, Phys. Rep. **437**, 125 (2007).
[65] J. A. McGovern, H. W. Griesshammer, D. R. Phillips, and D. Shukla, PoS CD **09**, 059 (2009).
[66] M. Kotulla, J. Ahrens, J. R. M. Annand, R. Beck, G. Caselotti, L. S. Fog, D. Hornidge, S. Janssen *et al*., Phys. Rev. Lett. **89**, 272001 (2002).
[67] M. Kotulla (TAPS/A2 Collaboration), Prog. Part. Nucl. Phys. **50**, 295 (2003).
[68] J. Linde and H. Snellman, Phys. Rev. D **53**, 2337 (1996).
[69] M. Kotulla, Prog. Part. Nucl. Phys. **61**, 147 (2008).
[70] M. Kotulla (TAPS and A2 Collaboration), Acta Phys. Polon. B **33**, 957 (2002).
[71] J. Beringer *et al*. (Particle Data Group Collaboration), Phys. Rev. D **86**, 010001 (2012).
[72] M. Dugger, B. G. Ritchie, J. P. Ball, P. Collins, E. Pasyuk, R. A. Arndt, W. J. Briscoe, I. I. Strakovsky *et al*., Phys. Rev. C **76**, 025211 (2007).
[73] J. Ahrens *et al*. (GDH and A2 Collaboration), Eur. Phys. J. A **21**, 323 (2004).
[74] R. A. Arndt, W. J. Briscoe, I. I. Strakovsky, and R. L. Workman, Phys. Rev. C **66**, 055213 (2002).